Hairpin-like optimal perturbations in plane Poiseuille flow

M. Farano, S. Cherubini, J.-C. Robinet, P. De Palma, Hairpin-like optimal perturbations in plane Poiseuille flow, J. Fluid Mech., Volume 775 , 25 July 2015 , R2 DOI: https://doi.org/10.1017/jfm.2015.320

Hairpin-like optimal perturbations in plane Poiseuille flow

Mirko Farano[1,2]†, Stefania Cherubini[2] Jean-Christophe Robinet[2] and Pietro De Palma[1]

[1]DMMM, Politecnico di Bari, Via Re David 200, 70125 Bari, Italy

[2]DynFluid Laboratory, Arts et Metiers ParisTech, 151 Boulevard de l'Hopital, 75013 Paris, France

(Received ?; revised ?; accepted ?. - To be entered by editorial office)

A very fast route to transition through the generation of hairpin vortices is unraveled using non-linear optimisation of initial perturbations to plane Poiseuille flow. Non-linear optimisations are performed for subcritical values of the Reynolds number, large initial energies and short target times, aiming at quickly trigger non-linear effects and generate self-sustained coherent structures. The obtained non-linear optimal solution is fully localized in space and constituted by large-amplitude thin vorticity tubes curved and tilted against the streamwise direction, able to turn very rapidly into a hairpin vortex. Analysing the perturbation shape along the principal axis of the localized vortical structure, we observe strong sweeps and ejections already at initial time. These alternating sweeps and ejections create the potential for an inflection instability occurring in a localized region away from the wall, generating the head of the primary and secondary hairpin structures, quickly inducing transition to turbulent flow.

Key words:

1. Introduction

Studying coherent structures in transitional and turbulent shear flows is fundamental to understand the nature of such complex flows. In fact, due to their long lifetime, coherent structures determine a large part of the mean properties of the flow, while their generation, instability, and sustainment mechanisms may be useful to explain many details of the dynamics of turbulent flows. Two main examples of coherent structures are streaks and hairpin vortices, which have been observed experimentally and numerically in channel flows, pipe flows, and boundary-layer flows (Matsubara & Alfredsson (2001); Adrian (2007); Wu & Moin (2009); Singer (1996)).

Streaky structures are observed at different scales in transitional and turbulent shear flows (Brandt.. Hwang & Cossu PRL..) and their origin seems now to be well understood. As conjectured by Landahl (1980) some decades ago, elongated near-wall zones of low or high momentum are created by a mechanism of transient growth of the perturbations known as lift-up effect. Such a mechanism is based on the transport of the mean shear by rolls of streamwise vorticity. Due to linear transient growth mechanisms such as the lift-up, an asymptotically stable shear flow can act as an amplifier of small-amplitude disturbances, producing an output mainly composed by the most amplified flow structures (Luchini (2000)). The quest for the origin of these coherent structures has

† Email address for correspondence: m.farano@libero.it

stimulated the search for perturbations providing maximum amplification in a finite 'target time', defined as "optimal perturbations". By optimizing the perturbation energy in a linear framework, several authors have found initial optimal disturbances corresponding to streamwise-elongated rolls inducing streamwise streaks at target time(Butler & Farrell (1992); Luchini (2000)). The shape of these optimal perturbations correspond well to coherent structures found in transitional turbulent turbulent flows (Luchini (2000)) in a low-to-moderate disturbance environment. Thus, streaky structures can be explained as the projection of flow disturbances onto the linear optimal flow structure.

Also the mechanism of formation of hairpin vortices has been extensively studied. Wu & Moin (2009) have analyzed the generation of hairpin structures from Lambda shaped vortex structures induced in a boundary layer by the receptivity process from large amplitude free stream turbulence; Acarlar & Smith (1987) and Wu & Moin (2009) studied the formation of hairpin vortices by localized disturbances in boundary-layer and channel flows, respectively. Suponitsky *et al.* (2005) have studied a simple model of interaction between a localized vortical disturbance and an uniform unbounded shear flow, showing that a small-amplitude initial disturbance always evolves into a streaky structure, whereas a large-amplitude one evolves into a hairpin vortex under some conditions. Furthermore, it is well established that hairpin vortices appear as the consequence of the secondary instability and break-up of elongated streaks (Schmid & Henningson (2001)) These studies indicate that, unlike streaky structures, hairpin vortices are generated through nonlinear interactions (Eitel-Amor *et al.* (2015)). The fact that they naturally arise in many transitional and turbulent shear flows, as the consequence of the instability of streaks or induced by other causes (such as roughness elements or flow injection at wall) suggests the existence of a strong energy growth mechanism triggered by non-linearity. Whether the hairpin vortex might be recognized as an optimal flow structure in a nonlinear energy growth process is the question we want to address in the present paper. At this purpose, we will perform nonlinear optimizations in a simple parallel shear flow such as the plane Poiseuille flow.

Nonlinear optimizations in parallel shear flows have been recently performed by Pringle *et al.* (2012); Cherubini *et al.* (2011); Cherubini & De Palma (2013); Monokrousos *et al.* (2011); Rabin *et al.* (2012) the pipe and the Couette flow. In both cases the nonlinear optimal perturbations were found to induce strongly bent streaks, but hairpin vortices have never been observed. However, in those works the optimizations were performed for rather long target times, at which the lift-up mechanism dominate the dynamics. In order to focus our optimization analysis on the phase of generation of the hairpin structure, we need to choose finite amplitude initial perturbations and small target times to rapidly trigger nonlinear effects. In particular, the chosen target time is typical of the Orr mechanism, much smaller than the typical scale of the lift-up mechanism.

The paper is organized as follows: in the second section we define the problem; in the third section we discuss the results; in the last section an outlook is provided.

2. Problem formulation

The plane Poiseuille flow in subcritical conditions is considered. Nondimensional variables are chosen such that half the distance between the plates is $h = 1$ and the centerline velocity of the laminar flow is $U_c = 1$. Dirichlet boundary conditions for the three velocity components are imposed at the wall, whereas periodicity is prescribed in the streamwise and spanwise directions (denoted x and z, respectively, whereas y denotes the wall-normal direction). The streamwise, wall-normal, and spanwise dimensions of the computional domain are 2π, 2, and π, respectively. It is discretized using a staggered grid

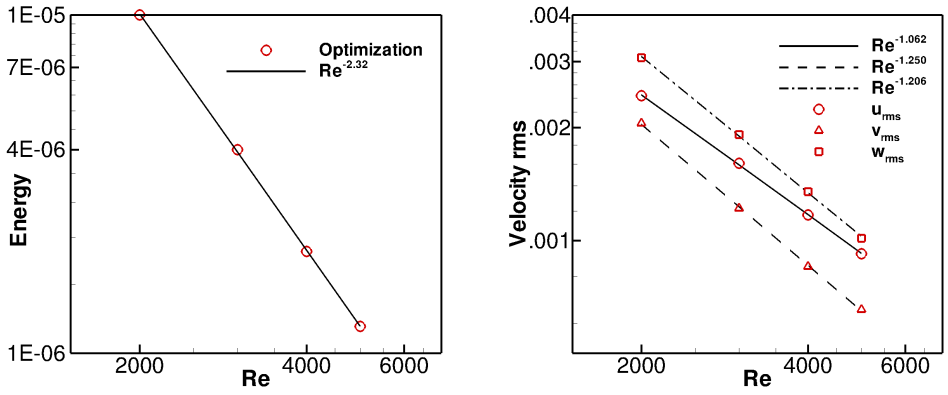

(a) E_{0min} (b) Velocity rms

FIGURE 1. Log-Log plot indicating the scaling law for the minimal energy density (a) and velocity amplitude (b) of such an highly non-linear optimal perturbation able to suddenly provide hairpin formation in subcritical transition.

with $300 \times 100 \times 120$ points. The Navier–Stokes equations are solved by a fractional-step method with second-order accuracy in space and time (Verzicco & Orlandi (1996)). The optimization procedure aims at computing the velocity perturbation $\mathbf{u} = (u, v, w)^T$ at $t = 0$ providing the maximum value of a chosen objective function at a given target time, T_{opt}. The chosen objective function is the ratio between the energy density at T_{opt} and the initial (given) one, where the energy density is defined as:

$$E(t) = \frac{1}{V}\int_V e\,(t)\,dV = \frac{1}{V}\int_V \frac{1}{2}(u^2 + v^2 + w^2)\,(t)\,dV. \tag{2.1}$$

The optimization problem is subject to partial differential constraints, namely the perturbative Navier-Stokes equations. Moreover, for the non-linear optimization, the initial value of the energy density must be imposed ($E(0) = E_0$). To optimize the chosen objective function subject to these constraints, a *Lagrange multiplier technique* is used coupled with an direct-adjoint iterative procedure using a *gradient-based method*. For further details on the optimisation algorithm the reader is referred to Cherubini *et al.* (2011).

3. Results

We perform non-linear optimizations of finite-amplitude three-dimensional perturbations for the plane Poiseuille flow focusing on subcritical values of the Reynolds number, namely, $Re = 2000, 3000, 4000, 5000$. In order to find optimal perturbations rapidly triggering coherent structures sustained by non-linear effects, we focus on the time scale of the Orr mechanism, which acts on time scales of order $\min(Re, \tilde{v}^{-1})$ (where $\tilde{v}$ represents the streamwise vortices amplitude, see Waleffe (1995)). Performing several linear optimisations, we have found that the transient energy growth due to the Orr mechanism peaks at $t \approx 10$ for all of the considered Reynolds numbers. It is noteworthy that such a time interval is smaller than the characteristic lift-up time scale. Thus, $T_{opt} = 10$ has been chosen for the following non-linear three-dimensional optimisations. Moreover, using this short target time, we must choose a sufficiently large initial energy density in order to trigger non-linear mechanisms. Thus, several non-linear optimisations have been

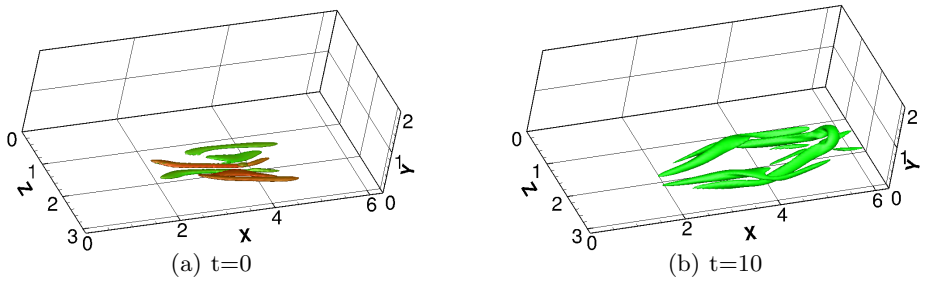

FIGURE 2. Isosurfaces of the Q-criterion for the non-linear optimal perturbation obtained with $T_{opt} = 10$ and $E_0 = 2 \times 10^{-6}$: (a) $t = 0$, $Q = 0.01$ and (b) $t = 10$, $Q = 0.2$.

performed increasing the value of E_0 until the energy gain at target time, $E(T)/E_0$, achieves a value larger than the linear energy gain, indicating that non-linear effects are non-negligible. This value of E_0 has been successively bisected in order to determine this *non-linearity threshold* with an accuracy of .. (X MIRKO: METTI ACCURATEZZA!!!) The values of this energy threshold are shown in Figure 1 (a) for all of the considered values of Re. These values appear well fitted by the scaling law $E_{0th} \propto Re^{-2.25}$. Corresponding thresholds on the rms velocity values are shown in figure 1 (b): the three velocity components are found to follow slightly different scaling laws, all of them with exponent close to -1. This fitting is consistent with different scaling laws of the form $\mathcal{A} \propto Re^{\gamma}$ proposed in the literature for fast subcritical transition induced by different initial disturbances, namely: i) $\gamma = -\frac{3}{2}$ for initial streamwise vortices (Chapman (2002)); ii) $\gamma = -\frac{5}{4}$ for initial oblique vortices; iii) $\gamma = -1$ for the Waleffe & Wang (2005) model; $\gamma = -\frac{3}{2}$ for wall-normal flow injection inducing hairpin vortices (Cohen *et al.* (2009)).
Figure 2 (a) shows the non-linear optimal perturbation obtained for $(Re, E_0) = (4000, 2 \times 10^{-6})$, which is composed by several thin tubes of counter-rotating vorticity alternated in the spanwise direction and fully localized in space, both in the streamwise and spanwise directions. The vortices are characterized by a large streamwise vorticity component and are tilted against the base flow, confirming the presence of linear energy growth mechanisms such as the lift-up (Landahl 1980) and the Orr (Orr 1907) mechanisms. However, this optimal solution is strongly different from linear optimals found for the same flow due to: i) its strong localization; ii) its smaller wavelength in the spanwise direction; iii) the presence of an inclination of the vortical structures in the spanwise direction. In particular, figure 2 (a) shows three pairs of vortices, all of them having different spanwise inclination and length, characterized by a streamwise vorticity of alternating sign. One can observe that the two inner pairs of vortices at the center of the structure are very close to each other. When such a structure evolves in time, a strong interaction of the vortices occurs immediately after the tilting in the stream wise direction. Therefore, a "hot spot" develops, which appears to be the seed of the hairpin vortex shown in figure 2 (b) at the target time. It is also noteworthy that, unlike other parallel shear flows, such as the Couette flow Cherubini & De Palma (2013), this non-linear optimal structure is characterized by a symmetry which is maintained when ithe initial energy E_0 is increased. We have verified that the optimal perturbation is characterized by this symmetry only at small target times; for target times typical of the lift-up mechanism, the optimal perturbation strongly resembles the one found in the Couette flow Cherubini & De Palma (2013). Figure 3 (a) clearly shows the symmetry of the streamwise and wall-normal velocity components, whereas the spanwise component is antisymmetric with respect to a $z-$constant axis, recalling the structure of varicose perturbations (Schmid & Henningson 2001). Moreover, it is worth noting that the streamwise and wall-normal

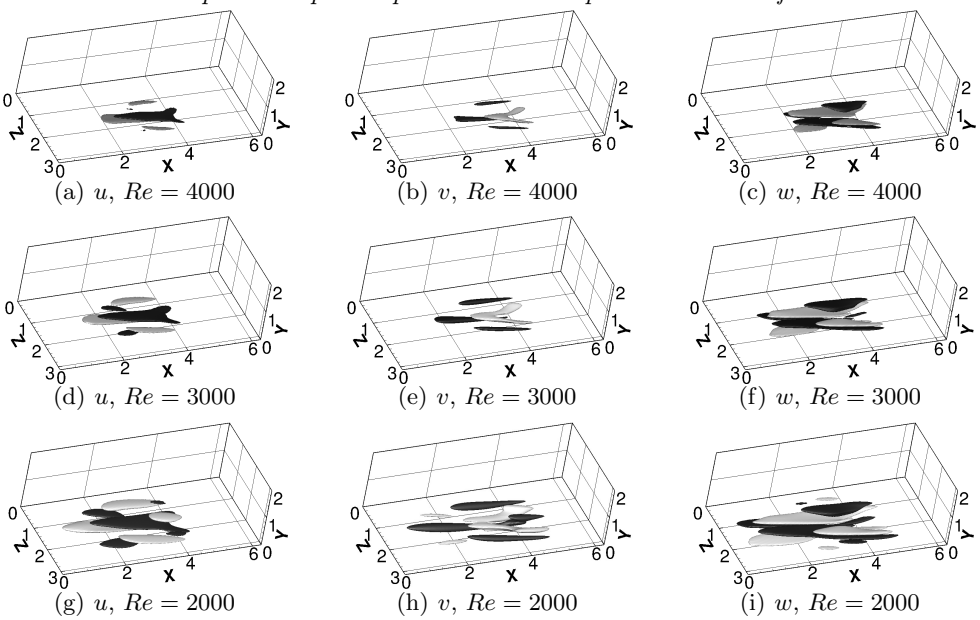

FIGURE 3. Isosurfaces of the three velocity components (light grey for positive and black for negative values, $u, v, w = \pm 0.01$) of the non-linear optimal perturbation for $T_{opt} = 10$ for different initial energy and Reynolds number: (top frames) $E_0 = 2 \times 10^{-6}$, $Re = 4000$, (middle frames) $E_0 = 4 \times 10^{-6}$, $Re = 3000$, and (bottom frames ($E_0 = 1 \times 10^{-5}$, $Re = 2000$).

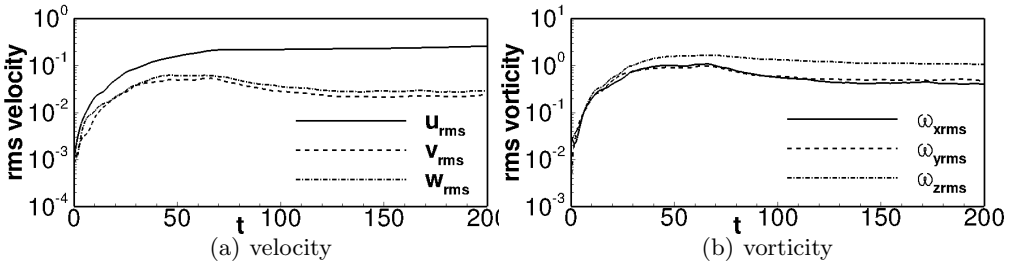

FIGURE 4. Evolution in time of velocity and vorticity rms for non-linear optimal perturbation with $E_0 = 2 \times 10^{-6}$ and $T_{opt} = 10$

components of the velocity clearly show a Λ structure oriented against the flow. This structure, once tilted by the Orr mechanism, becomes a precursor of the hairpin vortex. Very similar structures are found for different Reynolds numbers, as shown in figures 3 (d-i) for $Re = 2000, 3000$, although the latter perturbations are characterized by larger amplitudes (see the scaling in figure 1).

Direct numerical simulation (DNS) has been employed to study the time evolution of the initial optimal perturbations into a hairpin vortex and its subsequent transition to turbulence. The non-linear optimal perturbation computed at $Re = 4000$ for $E_0 = 2 \times 10^{-6}$, has been used to initialize the computation. The results are shown in figure 4 (a) and (b) providing the rms values of velocity and vorticity (respectively) versus time. It appears that all of the velocity and vorticity components grow together until reaching transition in a relatively short time (at $t \approx 50$). It is noteworthy that in other transition scenarios, such as oblique and streaks instability (see Schmid & Henningson (2001)), the streamwise velocity experiences a much larger growth than the other components.

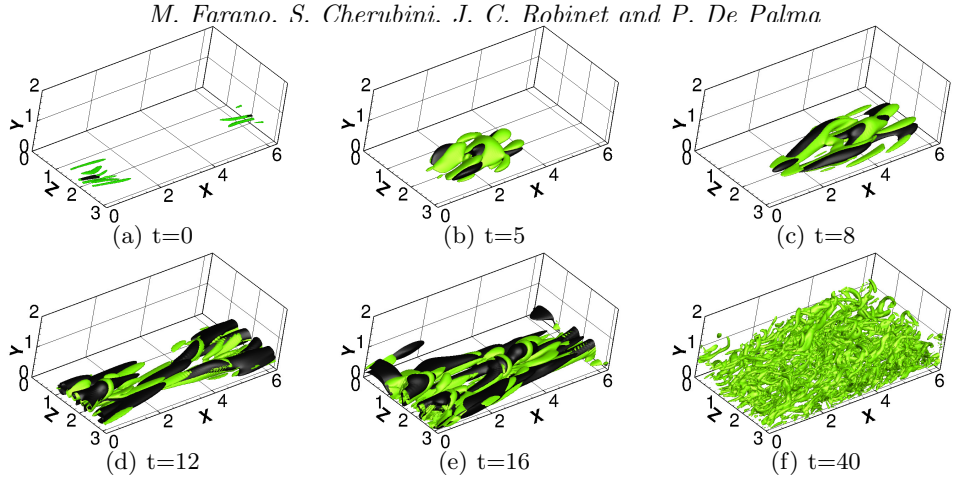

FIGURE 5. Evolution of non-linear optimal perturbation for $T_{opt} = 10$ and $E_0 = 2 \times 10^{-6}$. Isosurface of Q-criterion ((a-e) $Q = 0.02$; (f) $Q = 0.1$, green) and streamwise velocity disturbance ($u = -0.03$, black).

Snapshots of the time evolution of the vorticity (green) and of the negative streamwise velocity (black) are provided in figure 5. The initial vortex tubes are alternated in z and have opposite inclination with respect to the streamwise direction (see figure 5 (a)), so that the downstream tilting due to the Orr mechanism induces already at $t = 4$ the merging of two of these vortices in a tube of spanwise vorticity resembling a hairpin head (see frames (b)-(c)). Patches of positive and negative streamwise velocity can be observed in the flow; for $t \leqslant T_{opt}$ they appear rather localized in the streamwise direction (frame (c)) and they elongate in the streamwise direction, creating streaks, at times larger than the target time (frames (d-e)). It appears that the hairpin head is originated by a strong localized streamwise velocity defect (Adrian (2007)), which is rather large already at $t = 0$ (see the rms values in figure 1). This defect further increases its amplitude due to the Orr mechanism and to a *modified lift-up* mechanism (see Cherubini *et al.* (2011)) driven by the initial vortex filaments, until inducing local inflection points in the instantaneous velocity profile. To analyze how those defects are created, we have studied the evolution of the main vortical structures in time. Following Suponitsky *et al.* (2005), the coordinates of the center of the vortical structure (CVS) are defined by the following equation:

$$X_i = \frac{\int_V \|\overline{\omega}\|^2 x_i dV}{W}, \tag{3.1}$$

where $\overline{\omega}$ is the vorticity vector, $W = \int_V \|\overline{\omega}\|^2 dV$ is the enstrophy integral, and the index $i = 1, 2, 3$ indicates Cartesian components. To identify the spatial orientation of the vortical structure centered at X_i, we employ the tensor of enstrophy distribution (TED), defined as follows:

$$T_{ij} = \int_V \|\omega\|^2 (x_i - X_i)(x_j - X_j) dV, \tag{3.2}$$

Since the TED is a symmetric tensor, all its eigenvalues are real. The eigenvector associated with the largest eigenvalue identifies the direction of the *principal axis* of the vortex, along which the vortex has the largest extension. The insets in figures 6 (a) and (b) show by red lines the principal axis of the vortical structures (represented in green by the Q criterion surfaces) extracted from the DNS at $t = 5$ and $t = 10$, respectively. Being the flow structures mainly aligned with this direction, we evaluate along this axis

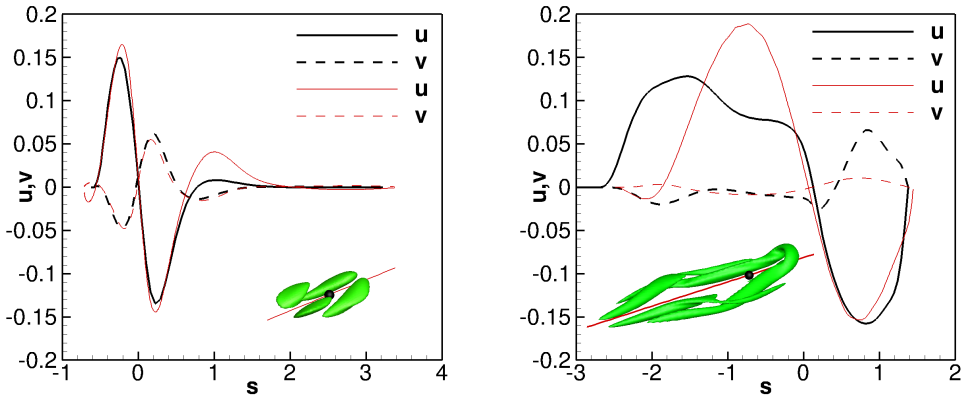

(a) t=5 (b) t=10

FIGURE 6. Velocity profile along the principal axis extracted at two different times from a fully non linear (black) and a linearized (red) DNS initialized by the non-linear optimal at $(Re, E_0) = (4000, 2 \times 10^{-6})$.

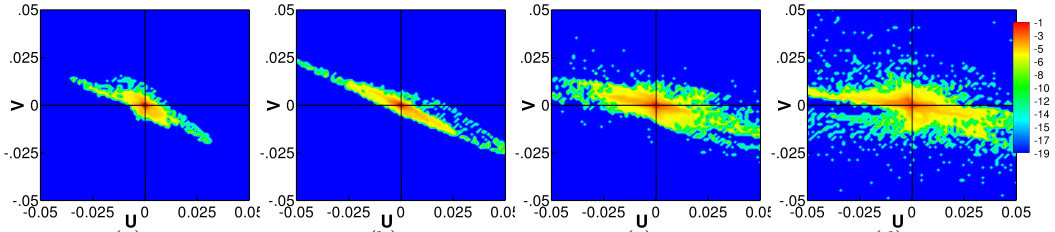

(a) t=0 (b) t=1 (c) t=6 (d) t=10

FIGURE 7. Contours of the logarithm of the probability density function of the wall-normal and streamwise velocity disturbance in a $u-v$ plane ($w = 0$) for $0 \leqslant y \leqslant 1$, extracted at $t = 0, 1, 6, 10$ from a DNS initialized with the non-linear optimal with $T_{opt} = 10$ and $E_0 = 2\times10^{-6}$. The values of the logarithm of the PDF has been normalized over the number of point of the computational domain.

the distribution of the streamwise and wall-normal velocity components. Figures 6 (a) and (b) show such distributions versus the abscissa s along the principal axis ($s = 0$ at the CVS) for two different times. At $t = 5$ (figure 6 (a)) we can observe that the velocity components u and v mostly have opposite sign and are equal to zero for $s = 0$. This behaviour recalls a fundamental feature of eddy motion in wall turbulence, namely, fluctuations have higher probability of spending time in the second (Q2) and fourth (Q4) quadrants of the $u - v$ plane (Adrian (2007)), inducing two kind of events: i) *ejections*, characterized by negative streamwise fluctuations lifted away from the wall by positive wall-normal fluctuations; ii) *sweeps*, characterized by positive streamwise fluctuations being moved toward the wall. To confirm such a similarity, we have computed the probability density function (PDF) of the perturbation velocity components at different times. Figure 7 shows the PDF values (in a logarithmic scale) of the streamwise and wall-normal components of the velocity perturbation, confirming the presence of ejections and sweeps already at $t = 0$, and up to the time of formation of the hairpin vortex. For instance, in Figure 6 (a) a sweep is observed upstream of the CVS ($s < 0$) followed by a strong ejection and a weak sweep downstream of the CVS ($s > 0$). At $t \approx 10$, the hairpin

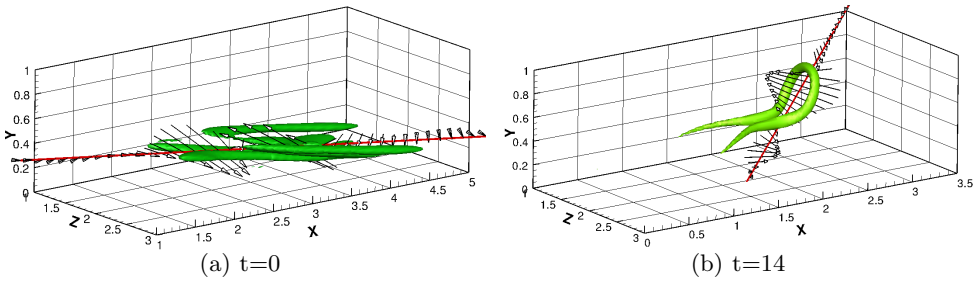

(a) t=0 (b) t=14

FIGURE 8. Wall-normal and streamwise vector component of velocity disturbance on an axis following the inclination of the main vortical structures for the non-linear optimal with $E_0 = 2 \times 10^{-6}$: (a) $t = 0$, (b) $t = 14$. Isosurface of the Q-criterion ((a) $Q = 0.01$, (b) $Q = 4$)

head is formed downstream of the CVS ($s > 0$), in correspondence with an ejection, as shown in figure 6 (b). This is not surprising since, as found in wall turbulence for a channel flow, the eddy associated to an ejection has a hairpin vortex shape (Adrian 2007). Comparing figure 6 (a) and (b), one can observe that when the hairpin head is formed, the zone of ejection increases its intensity, while the sweep region enlarges in the streamwise direction, reducing its intensity. When the evolution of the same initial perturbation is computed by a linearized DNS, the velocity distribution for $t > 5$ is characterized by increasing values of u and much lower values of v, as provided by the red lines in figure 6. Therefore, in the linearized case, larger streaks will be formed due to the lift-up effect but they will not be associated with wall-normal velocities of opposite signs, rapidly damping the ejection event that is responsible for the lifting of the hairpin head, thus preventing the creation of the hairpin structure. Figure 8 shows that the alternation of strong sweeps and ejections found at $t = 0$ is maintained at larger times, thus representing a basic element for the rapid hairpin formation. Moreover, in figure 8 (b) one can observe that the hairpin head is placed right in the zone of interaction of the stronger ejection with the stronger sweep, indicating that the formation of the spanwise vortex connecting the initial quasi-streamwise vortices might be a consequence of an inflectional instability taking place in this interaction zone. This observation is in agreement with the minimal flow-element model proposed by Cohen *et al.* (2014), in which a wavy spanwise vortex sheet was necessary to provide the inflection points for creating hairpin vortices from streamwise counter-rotating vortex pairs. Figure 9 (a) and (b) provide the instantaneous velocity and vorticity profiles at $t = 10$, computed solving the non-linear and the linearized Navier-Stokes equations, respectively, extracted along a vertical axis passing through the hairpin head in the non-linear case. In figure 9 (a) one can observe an inflection point, located at the point corresponding to the peak of vorticity measured at the hairpin head (at $y \approx 0.7$), in the outer zone of the velocity profile; whereas, in the near-wall region, at $y \approx 0.15$, one can observe the deformation of the velocity profile induced by the formation of a negative streak. The inflection point is observed in the linearized case as well (figure 9 (b)), but it is placed closer to the wall ($y \approx 0.4$), consistent with a shear layer instability induced by a streak. Moreover, in the non-linear case the vorticity peak moves in time towards to the center of the channel, reaching an amplitude one order of magnitude larger than that of the linearized case. Thus, the formation of the hairpin head appears essentially due to a local inflectional point induced by aternance of sweeps and ejections already present at the initial time and increasing in time. Non-linear effects appear necessary to sustain the coupling of the stream wise velocity component with the wall-normal one inducing the lifting of the hairpin head. When the head of the hairpin is pushed by the wall-normal perturbation

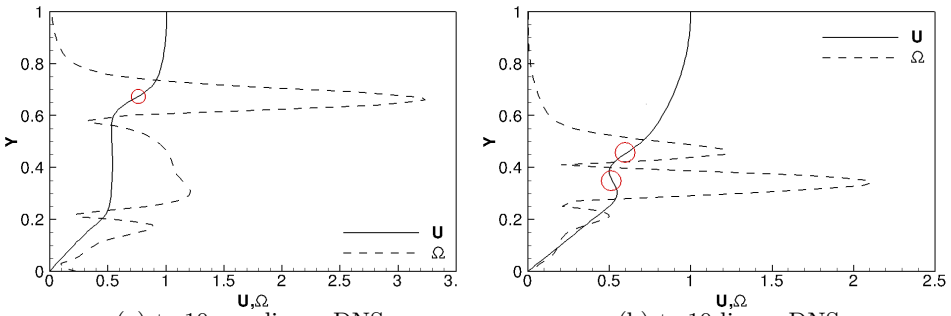

(a) t=10 non-linear DNS (b) t=10 linear DNS

FIGURE 9. Streamwise velocity and vorticity profiles at $t = 5$ along a wall-normal line passing through the hairpin head computed by the DNS (a) by the linearized DNS (b), initialized with the optimal for $E_0 = 2 \times 10^{-6}$.

toward the center of the channel, it is advected by the base flow at a higher velocity with respect to the part near the wall, stretching the whole vortical structure in the streamwise direction. Then, due to conservation of circulation, stretching provides a further growth of the vorticity, sustaining the hairpin vortex and allowing secondary hairpin structures to be created (Adrian 2007). The time evolution of the hairpin structure is visualized in figure 10, providing DNS snapshots showing isosurfaces of the Q-criterion (green), isolines of the streamwise velocity disturbance (red positive and black negative), and isocontours of the wall-normal velocity (white positive and black negative). One can notice the alternation of patches of u and v with different signs, spread all over the domain, and their effect on the lifting and stretching of the hairpin structure.

4. Outlook

Rapidly growing non-linear optimal perturbations have been computed for the plane Poiseuille flow, using small target times and finite initial energies. Such optimal perturbations are fully localized in space and characterized by spanwise-alternated thin tubes of counter-rotating vorticity inclined with respect to the streamwise direction. Transition is triggered suddenly and occurs in a very localized region, inducing very rapidly the formation of a hairpin structure. The initial optimal perturbation is characterized by localized sweeps and ejections inducing strong streamwise velocity defects which generate an inflectional point in the velocity profile. Inflectional instability thus create a spanwise vorticity tube that is lifted and stretched, generating the hairpin head.

The initial flow structure able to create a hairpin vortex in a very short time ($t \approx 10$) and then rapidly lead the flow to turbulence may be seen as an hairpin precursor, characterized by alternated sweeps and ejections of amplitude varying with Re^{-1}. It appears that, when non-linear effects are damped, the v components of the sweeps and ejections is not maintained, while the u components largely increase due to the lift-up mechanism, hampering the creation of the hairpin vortex and subsequent fast transition to turbulence. Thus, we have shown that, for the plane Poiseuille flow, a suitable combination of localized sweeps and ejections is capable of maximizing the energy growth in a short time interval generating an hairpin structure and transition towards turbulence. This optimal growth mechanism could be the reason why the final stage of transition to turbulence and turbulent boundary layer flows are characterized by a high density of hairpin structures.

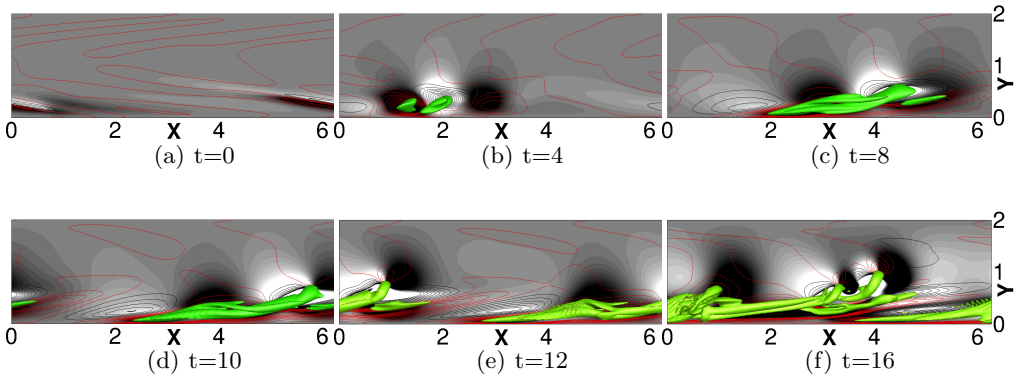

FIGURE 10. Evolution of non-linear optimal perturbation for $T_{opt} = 10$ and $E_0 = 2 \times 10^{-6}$. Slice $z = 2$. Isosurface of Q-criterion ($Q = 0.1$, green), isoline of streamwise velocity disturbance (red positive, black negative), and contours of wall-normal velocity disturbance (white positive, black negative).

Future works will aim at extending these findings for different shear flows, as well as for noisy or turbulent environments.

REFERENCES

ACARLAR, M. S. & SMITH, C. R. 1987 A study of hairpin vortices in a laminar boundary layer Part 2 Hairpin vortices generated by fluid injection . *J. Fluid Mech.* **175**, 43–48.

ADRIAN, RONALD J 2007 Hairpin vortex organization in wall turbulence. *Physics of Fluids (1994-present)* **19** (4), 041301.

BUTLER, KATHRYN M & FARRELL, BRIAN F 1992 Three-dimensional optimal perturbations in viscous shear flow. *Physics of Fluids A: Fluid Dynamics (1989-1993)* **4** (8), 1637–1650.

CHAPMAN, S. J. 2002 Subcritical transition in channel flows. *Journal of Fluid Mechanics* **451**, 35–97.

CHERUBINI, STEFANIA & DE PALMA, PIETRO 2013 Nonlinear optimal perturbations in a couette flow: bursting and transition. *Journal of Fluid Mechanics* **716**, 251–279.

CHERUBINI, STEFANIA, DE PALMA, PIETRO, ROBINET, J-C & BOTTARO, ALESSANDRO 2011 The minimal seed of turbulent transition in the boundary layer. *Journal of Fluid Mechanics* **689**, 221–253.

COHEN, J., KARP, M. & MEHTA, Y. 2014 A minimal flow-elements model for the generation of packets of hairpin vortices in shear flows . *J. Fluid Mech.* **747**, 30–43.

COHEN, J., PHILIP, J. & BEN-DOV, G. 2009 Aspects of linear and nonlinear instabilities leading to transition in pipe and channel flows. *Philosophical Transactions of the Royal Society A: Mathematical, Physical and Engineering Sciences* **367** (1888), 509–527.

EITEL-AMOR, G., ORLU, R., SCHLATTER, P. & FLORES, O. 2015 Hairpin vortices in turbulent boundary layers . *Phys. Fluids* **27**, 025108.

LANDAHL, MT 1980 A note on an algebraic instability of inviscid parallel shear flows. *Journal of Fluid Mechanics* **98** (02), 243–251.

LUCHINI, PAOLO 2000 Reynolds-number-independent instability of the boundary layer over a flat surface: optimal perturbations. *Journal of Fluid Mechanics* **404**, 289–309.

MATSUBARA, M & ALFREDSSON, P HENRIK 2001 Disturbance growth in boundary layers subjected to free-stream turbulence. *Journal of fluid mechanics* **430**, 149–168.

MONOKROUSOS, ANTONIOS, BOTTARO, ALESSANDRO, BRANDT, LUCA, DI VITA, ANDREA & HENNINGSON, DAN S 2011 Nonequilibrium thermodynamics and the optimal path to turbulence in shear flows. *Physical review letters* **106** (13), 134502.

ORR, WILLIAM M'F 1907 The stability or instability of the steady motions of a perfect liquid

and of a viscous liquid. part ii: A viscous liquid. In *Proceedings of the Royal Irish Academy. Section A: Mathematical and Physical Sciences*, pp. 69–138. JSTOR.

Pringle, Chris CT, Willis, Ashley P & Kerswell, Rich R 2012 Minimal seeds for shear flow turbulence: using nonlinear transient growth to touch the edge of chaos. *Journal of Fluid Mechanics* **702**, 415–443.

Rabin, SME, Caulfield, CP & Kerswell, RR 2012 Triggering turbulence efficiently in plane couette flow. *Journal of Fluid Mechanics* **712**, 244–272.

Schmid, Peter J & Henningson, Dan S 2001 *Stability and transition in shear flows*, , vol. 142. Springer.

Singer, Bart A 1996 Characteristics of a young turbulent spot. *Physics of Fluids (1994-present)* **8** (2), 509–521.

Suponitsky, Victoria, Cohen, Jacob & Bar-Yoseph, Pinhas Z 2005 The generation of streaks and hairpin vortices from a localized vortex disturbance embedded in unbounded uniform shear flow. *Journal of Fluid Mechanics* **535**, 65–100.

Verzicco, R & Orlandi, P 1996 A finite-difference scheme for three-dimensional incompressible flows in cylindrical coordinates. *Journal of Computational Physics* **123** (2), 402–414.

Waleffe, Fabian 1995 Transition in shear flows. nonlinear normality versus non-normal linearity. *Physics of Fluids (1994-present)* **7** (12), 3060–3066.

Waleffe, F. & Wang, J. 2005 Transition threshold and the self-sustaining process. In *IUTAM Symposium on Laminar-Turbulent Transition and Finite Amplitude Solutions*, pp. 85–106. Springer.

Wu, Xiaohua & Moin, Parviz 2009 Direct numerical simulation of turbulence in a nominally zero-pressure-gradient flat-plate boundary layer. *Journal of Fluid Mechanics* **630**, 5–41.